A Tabletop X-Ray Tomography Instrument for Nanometer-Scale Imaging: Demonstration of the 1,000-Element Transition-Edge Sensor Subarray

Paul Szypryt, Nathan Nakamura, Daniel T. Becker, Douglas A. Bennett, *Member, IEEE*, Amber L. Dagel, W. Bertrand Doriese, Joseph W. Fowler, Johnathon D. Gard, J. Zachariah Harris, Gene C. Hilton, Jozsef Imrek, Edward S. Jimenez, Kurt W. Larson, Zachary H. Levine, John A. B. Mates, D. McArthur, Luis Miaja-Avila, Kelsey M. Morgan, Galen C. O'Neil, Nathan J. Ortiz, Christine G. Pappas, Daniel R. Schmidt, Kyle R. Thompson, Joel N. Ullom, Leila Vale, Michael R. Vissers, Christopher Walker, Joel C. Weber, Abigail L. Wessels, Jason W. Wheeler, and Daniel S. Swetz

***Abstract*—We report on the 1,000-element transition-edge sensor (TES) x-ray spectrometer implementation of the TOMographic Circuit Analysis Tool (TOMCAT). TOMCAT combines a high spatial resolution scanning electron microscope (SEM) with a highly efficient and pixelated TES spectrometer to reconstruct three-dimensional maps of nanoscale integrated circuits (ICs). A 240-pixel prototype spectrometer was recently used to reconstruct ICs at the 130 nm technology node, but to increase imaging speed to more practical levels, the detector efficiency needs to be improved. For this reason, we are building a spectrometer that will eventually contain 3,000 TES microcalorimeters read out with microwave superconducting quantum interference device (SQUID) multiplexing, and we currently have commissioned a 1,000 TES subarray. This still represents a significant improvement from the 240-pixel system and allows us to begin characterizing the full spectrometer performance. Of the 992 maximimum available readout channels, we have yielded 818 devices, representing the largest number of TES x-ray microcalorimeters simultaneously read out to date. These microcalorimeters have been optimized for pulse speed rather than purely energy resolution, and we measure a FWHM energy resolution of 14 eV at the 8.0 keV Cu Kα line.**

***Index Terms*—Transition-edge sensors, superconducting microcalorimeters, multiplexing.**

I. Motivation

As INTEGRATED circuits (ICs) become more and more complex, with state-of-the-art ICs containing feature sizes of less than 10 nm, the challenge of three-dimensionally imaging fully fabricated ICs grows appreciably. This can be important for a number of purposes, including defect analysis during process development and verification of externally fabricated components. Although characterization techniques at nanoscales have been developed in a synchrotron setting [1], [2], [3], laboratory scale approaches [4], [5], [6] are a topic of active investigation and have not yet demonstrated the spatial resolutions of their beamline counterparts. Due to the relative sensitivity and value of ICs that require this sort of detailed mapping, however, a solution that is both tabletop and nondestructive is generally preferable in order to perform the measurement in-house and in a repeatable fashion.

The TOMographic Circuit Analysis Tool (TOMCAT; see [7]), which originated with the Non-destructive Statistical Estimation of Nanoscale Structures and Electronics (NSENSE; see [8], [9]) concept, was developed to address these issues. This tool combines a commercial scanning electron microscope (SEM) with a transition-edge sensor (TES; see [10], [11]) x-ray spectrometer in a tabletop tomography instrument. Unique to the TOMCAT approach is the deposition of the x-ray generating target layer (e.g. Pt) directly on the IC under test, with a spacer layer (e.g. Si) of carefully selected thickness between the target and IC layers used to set the magnification. The electron beam of the SEM is used to generate x-rays in a small region of the target layer, which then travel through the IC and are attenuated depending on local metal density and thickness. X-rays are detected with the TES spectrometer, which has sufficient energy resolution to discern characteristic x-rays generated at the target layer from background x-rays generated elsewhere (e.g. spacer and IC layers, vacuum chamber). Although a single metal slab target

Manuscript received 13 November 2022; revised 28 February 2023; accepted 7 March 2023. Date of publication 13 March 2023; date of current version 27 March 2023. This work was supported by the Office of the Director of National Intelligence (ODNI), Intelligence Advanced Research Projects Activity (IARPA), through the Rapid Analysis of Various Emerging Nanoelectronics (RAVEN) Research Program, under Grant D2021-2106170004. *(Corresponding author: Paul Szypryt).*

Paul Szypryt, Nathan Nakamura, Daniel T. Becker, Joseph W. Fowler, Johnathon D. Gard, Kelsey M. Morgan, Nathan J. Ortiz, Christine G. Pappas, Joel N. Ullom, Joel C. Weber, and Abigail L. Wessels are with the Department of Physics, University of Colorado, Boulder, CO 80309 USA, and also with the National Institute of Standards and Technology, Boulder, CO 80305 USA (e-mail: paul.szypryt@nist.gov).

Daniel R. Schmidt is with the National Institute of Standards and Technology, Boulder, CO 80305 USA.

Douglas A. Bennett, W. Bertrand Doriese, Gene C. Hilton, Zachary H. Levine, John A. B. Mates, Luis Miaja-Avila, Galen C. O'Neil, Leila Vale, Michael R. Vissers, and Daniel S. Swetz are with the National Institute of Standards and Technology, Boulder, CO 80305 USA.

Amber L. Dagel, J. Zachariah Harris, Edward S. Jimenez, Kurt W. Larson, D. McArthur, Kyle R. Thompson, Christopher Walker, and Jason W. Wheeler are with the Sandia National Laboratories, Albuquerque, NM 87185 USA.

Jozsef Imrek is with the National Institute of Standards and Technology, Boulder, CO 80305 USA, and also with the Theiss Research, La Jolla, CA 92037 USA.

Color versions of one or more figures in this article are available at https://doi.org/10.1109/TASC.2023.3256343.

Digital Object Identifier 10.1109/TASC.2023.3256343

has been used in all current TOMCAT measurements, a carefully designed nanopatterned target could also be used achieve x-ray generated spot sizes smaller than the electron beam spot size. Additionally, as TES microcalorimeters typically show part per thousand energy resolving power, the nanopatterned targets could also be constructed from multiple metals to *multiplex* the tomography measurement. As of this writing, TOMCAT has been used to reconstruct an IC with 6 logical layers (3 wiring and 3 via) and feature sizes as small as 160 nm [12]. Voxel sizes of 40 nm $\times$ 40 nm $\times$ 80 nm were used in this reconstruction.

Because there is only so much electron current that can be packed into a sufficiently small spot size, TOMCAT's imaging speed is ultimately limited by the spectrometer's x-ray collection capacity, namely the solid angle and detector speed. The original tomography scans were done with a prototype spectrometer containing 240 TES x-ray microcalorimeters [13] read out using superconducting quantum interference device (SQUID) based time-domain multiplexing (TDM; see [14]). In order to increase the imaging speed, we are developing a new spectrometer containing 3,000 TES x-ray microcalorimeters that are about 2.5$\times$ faster than the current devices, improvements largely made possible by microwave SQUID multiplexing (μMUX; see [15], [16]). Completion of the full 3,000-pixel system is expected in 2023, but at this time we have built up a 1,000-pixel subarray and integrated this smaller system with the rest of the TOMCAT instrument. The goals here are twofold. First, as the mechanical integration is more or less identical in the 3,000 and 1,000 pixel implementations, much of the integration risk is retired and we can gain an understanding of expected system performance. Second, the 1,000-pixel subarray already allows us to realize a substantial imaging speed increase ($\gtrsim 4\times$) over the original 240-pixel TDM system and can be used for tomography data collection while building the remainder of the system. This manuscript describes the 1,000-pixel implementation of the TOMCAT spectrometer, focusing on microcalorimeter characterization measurements that make useful predictions for the full 3,000-pixel spectrometer.

II. Spectrometer Design

The 3,000-pixel (and 1,000-pixel) spectrometer differs from the prototype 240-pixel spectrometer in a few main ways. First and foremost, it uses μMUX readout instead of TDM, providing considerably higher readout bandwidth totaling 24 GHz. Here, there are 6 parallel readout chains each operating from 4 GHz to 8 GHz. The designed resonator bandwidth of each channel (pixel) is 1 MHz, with approximately 7.5 MHz spacing between resonators. Second, we have developed compact and modular cryogenic detector and readout packaging, referred to as the *microsnout*, as shown in Fig. 1. Each microsnout contains a maximum of 256 detectors and associated cold readout components, and the 3,000-pixel instrument will use a total of 12 microsnouts arranged in a Swiss cross pattern. Each microsnout will use 2 GHz of readout bandwidth, and pairs of microsnouts (4 GHz to 6 GHz and 6 GHz to 8 GHz) will be daisy-chained together to form full readout chains. Finally, because the large detector array and cold readout electronics and wiring represent a much higher thermal load than the components in the 240-pixel spectrometer, the new spectrometer is housed in a dilution refrigerator instead of an adiabatic demagnetization refrigerator. On top of the higher cooling power of the dilution refrigerator, it has the advantage of continuous operation, further increasing data collection uptime. For a more detailed description of the 3,000-pixel spectrometer design, please see [17].

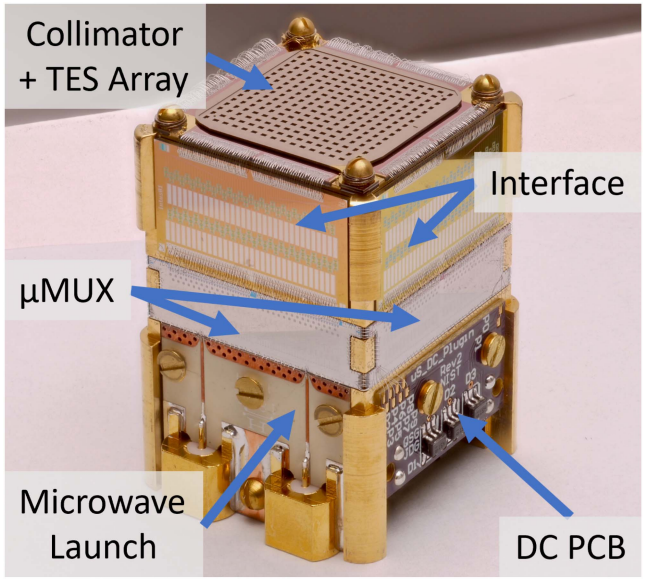

Fig. 1. Photograph of a microsnout used in the TOMCAT spectrometer. The TES microcalorimeter array is mounted to the top of the microsnout, and a collimator (aperture) array is used to ensure x-rays are only absorbed in the microcalorimeter absorbers. A set of 4 interface chips and 4 μMUX chips are used to bias and read out the TES microcalorimeter array. A microwave launch board and DC printed circuit board (PCB) are used to route the RF transmission line, flux ramp, and detector bias lines through the microsnout.

The 1,000-pixel subarray represents a scaled down version of the 3,000-pixel system and by and large follows the same design principles. The main difference is the 1,000-pixel instrument contains a 2 $\times$ 2 array of 4 microsnouts (central 4 microsnouts of the 12 microsnout Swiss cross pattern). Additionally, each of the 4 microsnouts is designed for the 4 GHz to 6 GHz band, so microsnouts are not daisy-chained together in this implementation, requiring slight modifications to the room temperature readout configuration. Finally, the vacuum windows and infrared filters are also not yet in their final implementation, temporarily reducing the system efficiency.

III. Characterization Measurements

We have begun characterizing the new TOMCAT spectrometer performance, particularly as it pertains to the 1,000-pixel implementation. We describe the performance of the cryogenic μMUX chips in Section III-A, the 1,000-pixel microwave readout in Section III-B, and the TES microcalorimeters in Section III-C.

A. μMUX Chip Performance

A microsnout contains 4 unique μMUX chips, each designed for a different 500 MHz wide subband of the full 4 GHz to 6 GHz range. Within a μMUX chip, there are 62 readout channels (rf-SQUID and resonator), for a total of 248 usable readout channels per microsnout. This is slightly smaller than the number of TES microcalorimeters (256) to allow for some flexibility in wiring around individual problematic devices while not exceeding the resources of the microwave electronics.

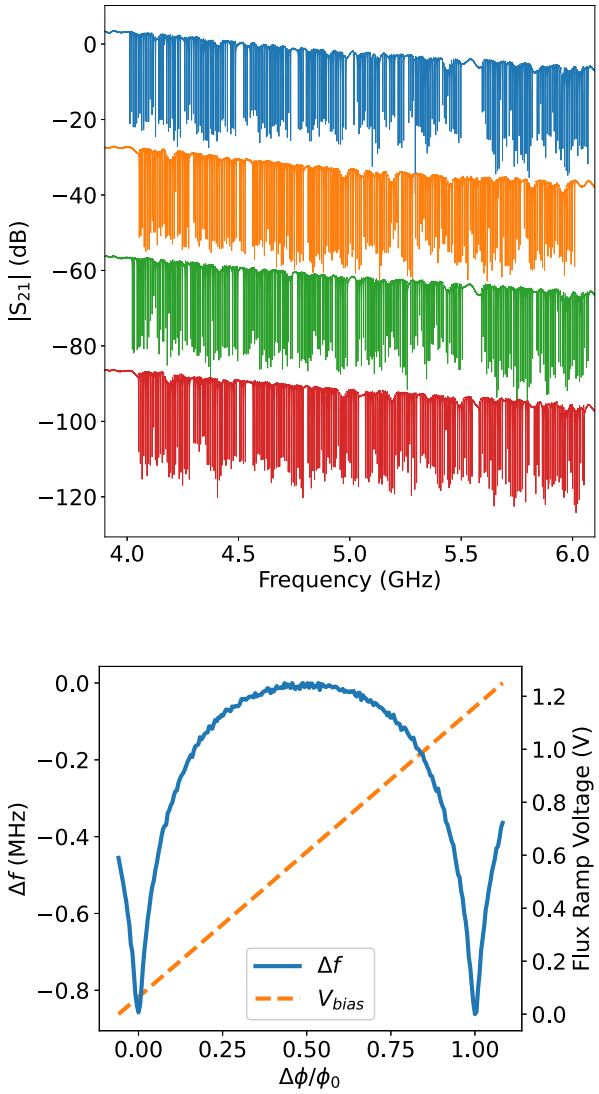

Fig. 2. (Top) Magnitude of the complex transmission for all 4 microsnouts, as measured with a VNA. The traces of the 4 microsnouts are offset by 30 dB steps, for clarity. A total of 967 good resonances were found in this sweep. (Bottom) Sample resonator response curve for a single readout channel when a flux ramp signal is applied to the rf-SQUID. A flux ramp amplitude of 1.1 V corresponds to a single SQUID period.

A vector network analyzer (VNA) was used to sequentially sweep the μMUX chips of all 4 microsnouts in the 3.9 GHz to 6.1 GHz frequency range, as shown see Fig. 2 (top). Of the $4 \times 248 = 992$ potential resonances, a total of 967 good resonances (frequency roughly in expected position and adequate separation between neighboring resonators) were measured with the VNA, for a working resonator yield of 97%. The VNA was also used to measure the resonator response to a flux ramp line voltage sweep on the rf-SQUIDs, as shown in Fig. 2 (bottom). The median frequency shift caused by biasing the SQUIDs across a flux quanta was measured to be −1.1 MHz, comparable to the design value of −1.4 MHz. An additional ∼20 readout channels were lost due to resonators showing no or negligible modulation from the flux ramp biased SQUIDs, or for instances when this modulation caused resonator overlaps (the uncertainty is from this latter effect and is attributed to small variations in operating conditions, such as from shifts in the magnetic field environment). This reduces the μMUX chip channel yield to 95%. This represents an average multiplexing factor of 237, the highest multiplexing factor achieved in TES-based x-ray microcalorimeter readout.

B. 4-Microsnout Readout Demonstration

In order to read out 4 microsnouts with the microwave electronics that were already available to us, we needed to alter the readout hardware configuration. In the 3,000-pixel setup, we will use a total of 6 readout enclosures, each containing a field programmable gate array and 4 intermediate frequency (IF) boards. Each IF board covers a 1 GHz frequency band (currently ∼ 950 MHz due to temporary firmware limitations), but there is flexibility in choosing the local oscillator (LO) frequency. A set of 4-way RF power combiners/splitters will be used to route the RF input/output signals of the 4 IF boards into a single microwave transmission line. For the 1,000-pixel implementation, we will split the resources of the readout enclosures to cover a pair of 4 GHz to 6 GHz bands rather than a single 4 GHz to 8 GHz band, which primarily involves a change to the LO frequencies and splitter/combiner setup. This way, we are able to utilize our 2 currently available enclosures for the readout of 4 microsnouts in the 4 GHz to 6 GHz band.

During the initial setup, the IF electronics are used to sequentially measure the the complex transmission through all 4 microsnouts and fit the center frequencies of all discovered resonators (at zero flux ramp voltage). The RF output tones are set to these frequencies. The amplitude of the flux ramp signal was set to create a $2\phi_0$ SQUID response across the flux ramp period, or 2.2 V. Although 16 samples are collected through a flux ramp period (4.096 μs), the first 8 samples are discarded to account for the flux ramp reset transient and only the latter 8 samples are used to track resonator phase response. A total of 951 readout channels were created during this tuning procedure, although many were incorrectly generated due to misidentified resonators and wiring shorts/opens, among other issues. Of these, 818 were found to have working detectors. Nevertheless, this is the largest number of TES x-ray microcalorimeters incorporated into a spectrometer and simultaneously read out to this date. The yield out of the 992 maximum readout channels was 82%. A histogram of the readout noise in each channel is shown in Fig. 3.

C. TES Microcalorimeter Characterization

In the TOMCAT design, the TES is a superconducting bilayer of MoAu with a target superconducting critical temperature of 100 mK [18]. The absorber is comprised of a 20 μm thick electroplated Bi layer, for high x-ray stopping power near 10 keV, on top of 2 μm thick Au layer, for lateral thermal conductance [19]. Due to the high expected count rates, the devices were optimized for fast recovery time instead of purely for energy resolution, done by increasing the thermal conductance between the TES and thermal bath.

During this initial set of measurements, the bath temperature was set to 50 mK and the detectors were voltage biased to a mean level of 25% of their normal state resistivity. We used the TOMCAT SEM to generate characteristic x-rays on the 4 microsnouts. X-rays were generated in the sample that was used in the tomography data collection described by [7] and [12], with x-rays generated in the 100 nm thick Pt target layer being of particular

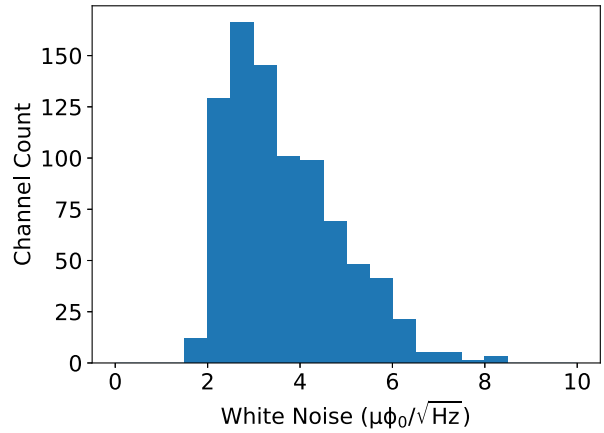

Fig. 3. Histogram of readout channel white noise levels, defined as the median noise level between 14.8 kHz to 16.8 kHz. Detector bias was zeroed prior to collecting noise data. For each channel, we averaged 100 individual spectra with a frequency resolution of 2 Hz. The plotted noise is referenced to the SQUID period, and the designed coupling is 10 $\mu A/\phi_0$. The median white noise level for these devices is 3.4 $\mu\phi_0/\sqrt{\text{Hz}}$, which degrades the resolution predicted from the filter signal-to-noise ratio at 8.0 keV by less than 0.6 eV.

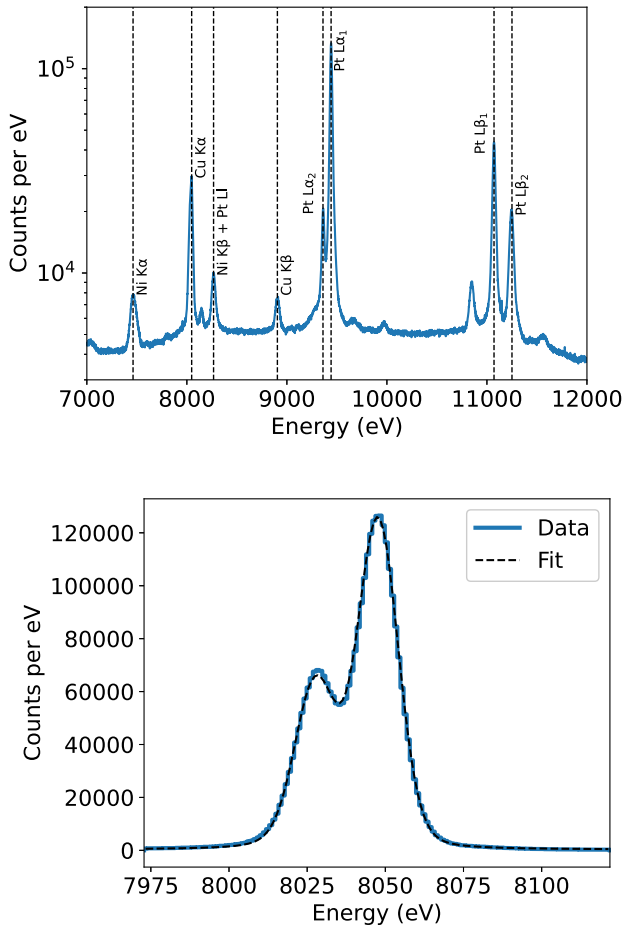

Fig. 4. (Top) Coadded energy spectrum of SEM generated x-rays. The main spectral feature associated with the target layer are the Pt Lα lines near 9.4 keV and Pt Lβ lines near 11 keV. These features are clearly resolvable from lines generated elsewhere in the sample (e.g. Cu Kα at 8.0 keV) or stainless steel chamber (Fe, Cr, and Ni Kα and Kβ lines between 5.4 keV to 8.3 keV). (Bottom) Fit to the Cu Kα feature in the coadded spectrum generated with external calibration source x-rays. A FWHM energy resolution of 14 eV was extracted from the fit parameters.

importance. The per pixel count rate (∼40 counts/pixel/s) was nearly identical to that observed with the previous 240-pixel spectrometer under the same SEM conditions, expected for the current IR filter and vacuum window configuration. The average pulse of each detector was examined to extract a median peak time of 40 μs and 1/e fall time of 180 μs. Because the Pt L line structure is not known well enough to characterize detector resolution, we also used an external x-ray calibration tube source with a Cu foil target at count rates similar to that of the SEM data collection. We used the Microcalorimeter Analysis Software System (MASS; see [20], [21]) to convert the x-ray pulse traces to energy values. Of the initial 818 channels that were analyzed in MASS, an additional 27 were cut due to anomalous count rates or pulse shapes. A broadband energy spectrum generated with the SEM x-rays is shown in Fig. 4 (top) and a fit to the Cu Kα line generated with the tube source x-rays is shown in Fig. 4 (bottom). A FWHM energy resolution of 14 eV was extracted from the Cu Kα fit (x-ray energy ∼8.0 keV). We note that the energy resolution predicted from the signal-to-noise ratio in the optimal filters is nearly identical in the x-rays generated by the SEM and tube source, so we do not expect degradation in achieved resolution when integrating the cryostat with the SEM.

IV. Conclusion and Future Work

We have demonstrated the readout of a kilopixel scale TES array intended for the TOMCAT experiment. The maximum number of readout channels as set by the μMUX hardware is 992, and of these a total of 818 channels had working devices, for a yield of 82%. This is the largest number of TES x-ray microcalorimeters simultaneously read out to date. A FWHM energy resolution of 14 eV was measured at the Cu Kα line using an external calibration source. The final full-scale instrument is still in construction, but it will roughly double the potential achievable multiplexing factor (248 to 496) and triple the maximum detector count (992 to 2976). This will be an extremely powerful tool for microcircuit tomography and will undoubtedly have applications across x-ray measurement science.

Acknowledgment

The authors would like to thank Eugene Lavely, Adam Marcinuk, Paul Moffitt, Steve O'Neill, Thomas Stark, Chris Willis and others at BAE Systems for their role in the NSENSE concept development and initial instrument integration in the NIST Boulder laboratories. The views and conclusions contained herein are those of the authors and should not be interpreted as necessarily representing the official policies or endorsements, either expressed or implied, of the ODNI, IARPA, or the U.S. Government Sandia National Laboratories is a multimission laboratory managed and operated by National Technology & Engineering Solutions of Sandia, LLC, a wholly owned subsidiary of Honeywell International Inc., for the U.S. Department of Energy's National Nuclear Security Administration under Contract DE-NA0003525, SAND No: SAND2022-13093.

REFERENCES

[1] G. Xu et al., "Nanometer precision metrology of submicron Cu/SiO_2 interconnects using fluorescence and transmission X-ray microscopy," *J. Appl. Phys.*, vol. 94, no. 9, pp. 6040–6049, Nov. 2003.

[2] M. Holler et al., "High-resolution non-destructive three-dimensional imaging of integrated circuits," *Nature*, vol. 543, no. 7645, pp. 402–406, Mar. 2017.

[3] Y. Jiang et al., "Achieving high spatial resolution in a large field-of-view using lensless X-ray imaging," *Appl. Phys. Lett.*, vol. 119, no. 12, Sep. 2021, Art. no. 124101.

[4] D. Kalasová et al., "Characterization of a laboratory-based X-ray computed nanotomography system for propagation-based method of phase contrast imaging," *IEEE Trans. Instrum. Meas.*, vol. 69, no. 4, pp. 1170–1178, Apr. 2020.

[5] F. Lutter et al., "Combining X-ray nano tomography with focused ion beam serial section imaging application of correlative tomography to integrated circuits," *Nucl. Instruments Methods Phys. Res. Sect. B: Beam Interact. Mater. At.*, vol. 500–501, pp. 10–17, Aug. 2021.

[6] D. Müller, J. Graetz, A. Balles, S. Stier, R. Hanke, and C. Fella, "Laboratory-based nano-computed tomography and examples of its application in the field of materials research," *Crystals*, vol. 11, no. 6, Jun. 2021, Art. no. 677.

[7] N. Nakamura et al., "A Tabletop X-Ray tomography instrument for nanometer-Scale imaging: Integration of a scanning electron microscope with a transition-Edge sensor spectrometer," 2022, *arXiv:2212.10591*.

[8] E. M. Lavely et al., "Nondestructive sample imaging," U.S. Patent 10468230, Nov. 2019.

[9] P. B. Weichman and E. M. Lavely, "Fluorescent X-ray scan image quality prediction," *J. Hardware Syst. Secur.*, vol. 4, no. 1, pp. 13–23, Mar. 2020.

[10] K. D. Irwin, G. C. Hilton, D. A. Wollman, and J. M. Martinis, "X-ray detection using a superconducting transition-edge sensor microcalorimeter with electrothermal feedback," *Appl. Phys. Lett.*, vol. 69, no. 13, pp. 1945–1947, Sep. 1996.

[11] K. D. Irwin and G. C. Hilton, "Transition-Edge sensors," in *Cryogenic Particle Detection*, (Series Topics in Applied Physics), C. Enss, Ed, vol. 99. Berlin, Heidelberg, Germany: Springer, 2005.

[12] Z. H. Levine et al., "A tabletop X-ray tomography instrument for nanometer-Scale imaging: Reconstructions," *Microsyst. Nanoeng.*, to be published.

[13] C. G. Pappas et al., "A TES X-ray spectrometer for NSENSE," in *Proc. GOMACTech*, 2019, pp. 300–305.

[14] W. B. Doriese et al., "Developments in time-division multiplexing of X-ray transition-edge sensors," *J. Low Temp. Phys.*, vol. 184, no. 1-2, pp. 389–395, Jul. 2016.

[15] J. A. B. Mates et al., "Simultaneous readout of 128 X-ray and gamma-ray transition-edge microcalorimeters using microwave SQUID multiplexing," *Appl. Phys. Lett.*, vol. 111, no. 6, Aug. 2017, Art. no. 62601.

[16] J. D. Gard et al., "A scalable readout for microwave SQUID multiplexing of transition-edge sensors," *J. Low Temp. Phys.*, vol. 193, no. 3/4, pp. 485–497, Nov. 2018.

[17] P. Szypryt et al., "Design of a 3000-pixel transition-edge sensor X-ray spectrometer for microcircuit tomography," *IEEE Trans. Appl. Supercond.*, vol. 31, no. 5, Aug. 2021, Art. no. 2100405.

[18] J. C. Weber et al., "Development of a transition-edge sensor bilayer process providing new modalities for critical temperature control," *Supercond. Sci. Technol.*, vol. 33, no. 11, Nov. 2020, Art. no. 115002.

[19] D. Yan et al., "Eliminating the non-gaussian spectral response of X-ray absorbers for transition-edge sensors," *Appl. Phys. Lett.*, vol. 111, no. 19, Nov. 2017, Art. no. 192602.

[20] J. W. Fowler et al., "The practice of pulse processing," *J. Low Temp. Phys.*, vol. 184, no. 1-2, pp. 374–381, Jul. 2016.

[21] D. T. Becker et al., "Advances in analysis of microcalorimeter gamma-ray spectra," *IEEE Trans. Nucl. Sci.*, vol. 66, no. 12, pp. 2355–2363, Dec. 2019.